JOURNAL OF SOLID STATE CHEMISTRY 93, 556–566 (1991)

Electronic and Spin State of High-Valent Iron Oxides Studied by a DV-Xα Cluster Method

H. ADACHI* AND M. TAKANO†

Hyogo University of Teacher Education, Yashiro, Hyogo 673-14, Japan; and †Institute for Chemical Research, Kyoto University, Uji, Kyoto-fu 611, Japan

Received December 17, 1990; in revised form April 22, 1991

The electronic and spin states of oxides containing highly charged Fe ions have been investigated by means of a DV-Xα cluster method. To study $CaFe^{4+}O_3$ and $SrFe^{4+}O_3$ in particular, model clusters FeO_6^{8-}, $A_8FeO_6^{8+}$ (A = Ca and Sr), and $Fe_2O_{11}^{14-}$ have been used, each being embedded in an appropriate Madelung potential. The direct contribution of the A cations to the valence state is almost insignificant. A covalent $O^{2-} \rightarrow Fe^{4+}$ electron transfer considerably reduces the effective charges of these ions. A high-spin state of a typical $d\uparrow^{4.44}d\downarrow^{0.77}$ configuration is stabilized. The exchange interaction between a pair of Fe ions is predicted to change its sign from ferromagnetic to antiferromagnetic above a critical Fe–O distance of ~1.93 Å. In a model cluster $Fe_2O_{11}^{14-}$ made of two octahedra having different Fe–O bond lengths, a partial charge and spin transfer from the Fe ion in the contracted octahedron to the other in the expanded octahedron takes place, thus explaining the disproportionation transition of $CaFeO_3$ formally expressed as $2Fe^{4+} \rightleftarrows Fe^{3+} + Fe^{5+}$.

Introduction

Transition metals can be stabilized in their unusual, high and low, valent states in perovskite-type oxides. In most of its oxides, for example, iron exists as ferric (Fe^{3+}) or ferrous (Fe^{2+}) ions, while the oxidation state is increased to 4+ in perovskites like $CaFeO_3$ and $SrFeO_3$ (*1–3*). The valence electronic state of these Fe^{4+} compounds has been investigated through the hyperfine interactions measured by the Mössbauer effect (ME) (*4–6*) and also through the magnetic moment estimated from neutron diffraction (*7*) and magnetization (*8*). However, $SrFeO_3$ and $CaFeO_3$ behave differently as seen from the low temperature ME data suggesting a strong composition dependence of the physical properties. At room temperature each $SrFeO_3$and $CaFeO_3$ shows a single component in the ME spectrum with a center shift (CS) characteristic of the Fe^{4+} state. Below 290 K, however, two components with the same intensities but with considerably different parameter values (including a magnetic hyperfine field (Hi) below T_N = 116 K) have been observed for $CaFeO_3$ (*9, 10*), while $SrFeO_3$ only shows a single component whose CS and Hi are intermediate between those for the double components of $CaFeO_3$. Thus, a second-order disproportionation transition ex-

* To whom correspondence should be addressed.

0022-4596/91 $3.00

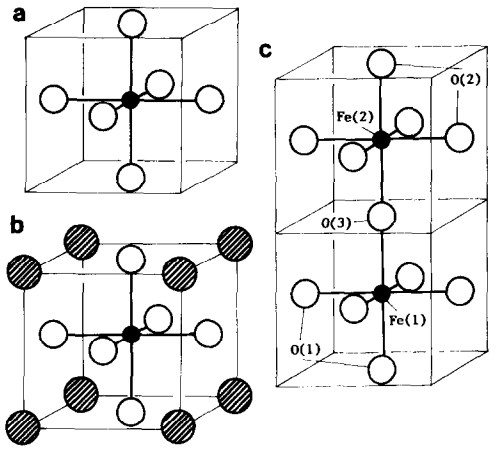

FIG. 1. Model clusters used for calculations. (a) FeO_6^{n-}, (b) $A_8FeO_6^{8+}$ (A = Ca and Sr), and (c) $Fe_2O_{11}^{14-}$. Open circles denote oxygen, closed circles iron, and shaded circles cation A.

pressed as $2Fe^{4+}(t_{2g}^3\sigma^{*1}) \rightleftarrows Fe^{3+}(t_{2g}^3e_g^2) + Fe^{5+}(t_{2g}^3)$ has been proposed for $CaFeO_3$ (*5, 6*). This explains the semiconductive behavior of $CaFeO_3$ in contrast with the metallic behavior of $SrFeO_3$. It has automatically been presumed, though not experimentally confirmed yet, that the transition is accompanied by quenching of the breathing phonon mode, that is, every second FeO_6 octahedron containing Fe^{3+} is expanded and the other containing Fe^{5+} contracted. A delicate balance between the electronic Fe–O–Fe interactions which make the σ^* band stable and the electron–phonon interactions which induce the disproportionation has thus been suggested (*11*).

In the present work, molecular cluster calculations using a spin-polarized DV-Xα method (*12, 13*) are performed to study the electronic and spin state of Fe^{4+} ions in perovskite oxides. We first illustrate the general features of Fe^{2+}, Fe^{3+}, Fe^{4+}, and Fe^{5+} ions by changing the charge of a model cluster FeO_6^{n-}. The electronic structure of Fe^{4+} is studied in more detail as a function of the Fe–O bond length. Utilizing a dimeric $Fe_2O_{11}^{14-}$ cluster made of a pair of octahedra sharing a bridging oxygen ion, we study the exchange interaction for various Fe–O distances and also discuss the quenched breathing mode model by allotting different Fe–O distances to the pair of octahedra.

Computational Method

The molecular orbitals of the model cluster FeO_6^{n-} (n = 10, 9, 8, and 7 for nominal Fe valences of +2, +3, +4, and +5, respectively) and $Fe_2O_{11}^{14-}$ (for nominal Fe^{4+} ions) shown in Figs. 1a and 1c were calculated by a DV-Xα method. Details of this method were described elsewhere (*12–14*). The Slater exchange parameter α was fixed at 0.7 for all the calculations. The numerical atomic orbitals obtained by solving the Shrödinger equation for the constituent atoms were used as the basis functions of

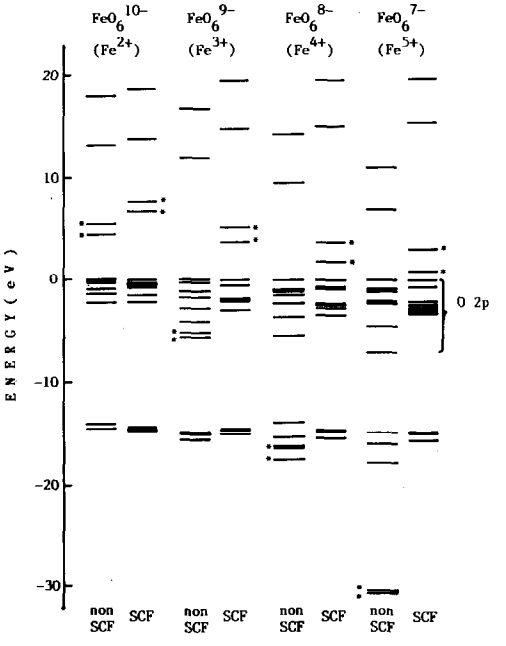

FIG. 2. Valence level structures for the FeO_6^{n-} clusters (see text).

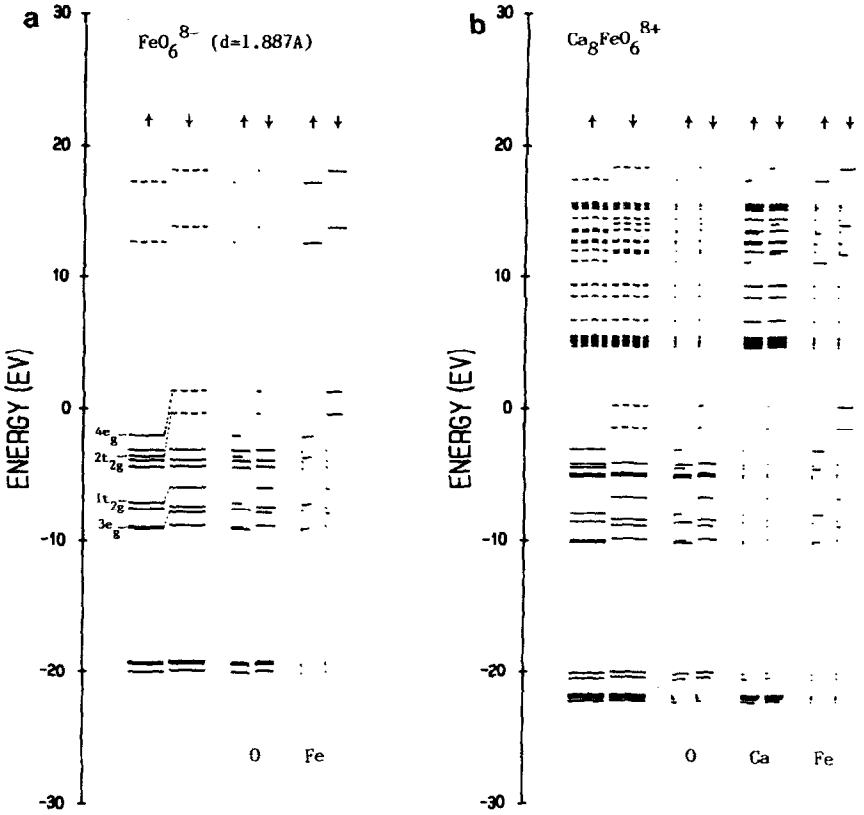

FIG. 3. Comparison of the level structures for FeO_6^{8-} and $Ca_8FeO_6^{8+}$ and the atomic components. Levels with up- and down-spin are indicated by ↑ and ↓, respectively. Occupied levels are indicated by solid lines and unoccupied ones by dotted lines.

the LCAO molecular orbitals. The basis set comprises the Fe 1*s*–4*p*, O 1*s*–2*p*, Ca 1*s*–4*p*, and Sr 1*s*–5*p* orbitals. By Mulliken population analysis ionicity and covalency were estimated from the molecular charge density of the clusters. Both spin-polarized and spin-restricted calculations were made to clarify the spin state and the magnetic interactions.

O_h symmetry was assumed for the single FeO_6^{n-} clusters. The Fe–O distance was varied with n using the ionic radii listed in Ref. (*15*). For cubic $SrFeO_3$ the Fe–O distance of $d = 1.925$ Å is appropriate. On the other hand, for $CaFeO_3$, which shows an incompletely specified tetragonal distortion ($a = 5.325$ Å, $c = 7.579$ Å), half the cubic root of the unimolecular cell volume, 1.887 Å, may tentatively be used as the d value. In order to investigate the influence of the countercations, Ca^{2+} and Sr^{2+}, on the valence state, calculations were done also for clusters $Ca_8FeO_6^{8+}$ and $Sr_8Fe_6O^{8+}$ shown in Fig. 1b to examine their orbital components in the valence levels.

In the $Fe_2O_{11}^{14-}$ cluster with C_{4v} symmetry two octahedra share one oxygen atom. We have looked into the detailed electronic and spin state of the Fe^{4+} ions and also the magnetic interaction between them as a function of d varying from 1.875 to 1.982 Å. As a model of the quenched breathing phonon

TABLE I
MULLIKEN POPULATION ANALYSIS FOR FeO_6^{n-} CLUSTERS

	FeO_6^{10-} (Fe^{2+})	FeO_6^{9-} (Fe^{3+})	FeO_6^{8-} (Fe^{4+})	FeO_6^{7-} (Fe^{5+})
	(i) Electron density			
O				
2*s*	1.987	1.978	1.972	1.970
2*p*	5.974	5.893	5.758	5.597
Net charge	−1.961	−1.871	−1.730	−1.566
Fe				
3*d*	6.273	5.751	5.475	5.344
4*s*	0.040	0.054	0.088	0.123
4*p*	−0.083	−0.039	0.047	0.127
Net charge	+1.765	+2.227	+2.381	+2.397
	(ii) f_p			
e_g	0.060	0.158	0.280	0.378
t_{2g}	0.017	0.055	0.138	0.253

mode, different Fe–O distances $d_1 = d + \Delta$ and $d_2 = d - \Delta$ were allotted to the two octahedra. The value d was fixed at 1.887 Å, while Δ was varied from 0.027 to 0.106 Å.

All the clusters employed in the present calculations were embedded in the Madelung-type electrostatic potential constructed by surrounding ions located at the lattice points of the perovskite structure (*14*).

Results and Discussion

First, we study the level structures of the FeO_6^{n-} clusters as a function of n. The valence levels calculated without considering spin polarization are indicated in Fig. 2. In the figure "non SCF" means calculations made for an illustrative purpose using purely ionic potentials of Fe^{m+} and O^{2-} ions ($m = 12 - n$), while "SCF" indicates self consistent calculations in which a covalent electron transfer occurs. Levels consisting mainly of Fe 3*d* components are marked by asterisks. These are split into two, t_{2g} and e_g, in an octahedral field. The non-SCF calculations show that the Fe 3*d* levels are lowered quickly as the oxidation number m increases so that those for $m \geqq 3+$ are located below the O 2*p* band. More realistically, a covalent electron transfer from O^{2-} to Fe^{m+}, which becomes more important as m increases, occurs. The final SCF levels thus containing certain amounts of O 2*p* components are shifted above the "O 2*p*" band. We denote the mixing ratio of the O 2*p* component in a "3*d*" level by f_p, which is a useful measure of the covalent interaction. The results of the Mulliken population analysis are summarized in Table I. The considerable reduction of the effective charges and

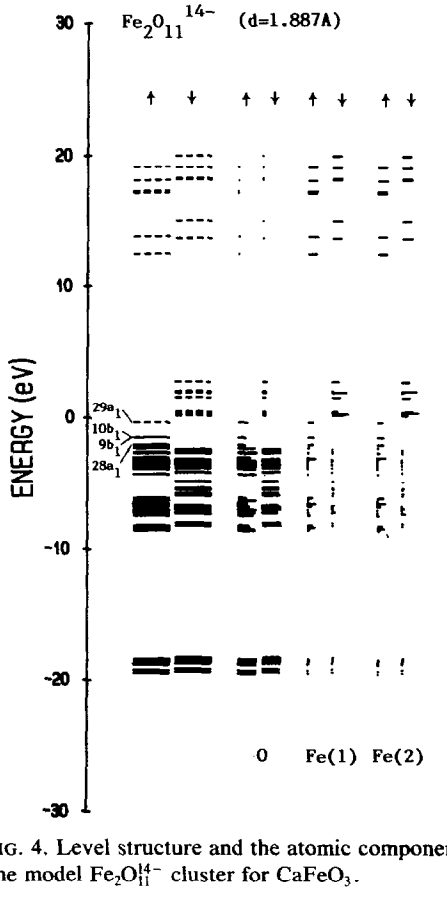

FIG. 4. Level structure and the atomic components of the model $Fe_2O_{11}^{14-}$ cluster for $CaFeO_3$.

TABLE II
MULLIKEN POPULATION ANALYSIS FOR VARIOUS $Fe_2O_{11}^{14-}$ CLUSTERS

	d = 1.887 Å		d = 1.925 Å		d_1 = 1.940 Å, d_2 = 1.834 Å			
	Fe (1, 2)		Fe (1, 2)		Fe(1)		Fe(2)	
	↑	↓	↑	↓	↑	↓	↑	↓
3*d*	4.443	0.768	4.469	0.780	4.723	0.585	4.166	0.974
4*s*	0.021	−0.009	0.035	0.005	0.025	−0.005	0.013	−0.013
4*p*	0.012	−0.035	0.026	−0.019	0.012	−0.037	0.006	−0.037
Net charge	+2.787		+2.699		+2.687		+2.877	
	O(1, 2)		O(1, 2)		O(1)		O(2)	
	↑	↓	↑	↓	↑	↓	↑	↓
2*s*	0.981	0.980	0.981	0.981	0.984	0.981	0.978	0.980
2*p*	2.957	2.905	2.948	2.897	2.990	2.925	2.922	2.886
Net charge	−1.823		−1.807		−1.880		−1.766	
	O(3)		O(3)		O(3)			
	↑	↓	↑	↓	↑	↓		
2*s*	0.985	0.977	0.984	0.977	0.985	0.977		
2*p*	2.678	2.710	2.654	2.697	2.690	2.686		
Net charge	−1.349		−1.313		−1.338			

TABLE III
THEORETICAL AND EXPERIMENTAL MÖSSBAUER PARAMETERS AND LOCAL MAGNETIC MOMENTS

	$CaFeO_3$			$SrFeO_3$
	d = 1.887 Å	d_1 = 1.974 Å,	d_2 = 1.834 Å	d = 1.925 Å
CS(mm/sec)	0.03	0.10	0.00	−0.01
	(0.16)[c]	(0.32)	(0.00)	(0.146)
Hi(T)	39.0	45.7	35.0	38.5
	(35.2)[c]	(41.9)	(28.4)	(33.1)
$\mu(\mu_B)$[b]	3.68	4.14	3.19	3.69
				(3.73)

[a] Experimental data are indicated in parentheses.
[b] Local moment estimated from the *d* electron spin density listed in Table II.
[c] Experimental values are the averages over the two kinds of Fe ions in $CaFeO_3$.

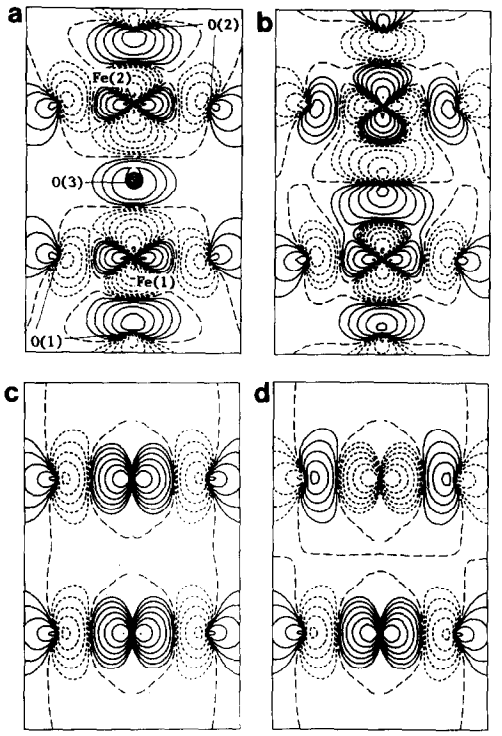

FIG. 5. Contour maps of the cluster wave functions on the (100) plane of the $Fe_2O_{11}^{14-}$ cluster. Two Fe ions and seven O ions are illustrated. (a) $28a_1\uparrow$, (b) $29a_1\uparrow$, (c) $9b_1\uparrow$, and (d) $10b_1\uparrow$.

the strong Fe $3d$–O $2p$ mixing represent the strong covalency in the "Fe^{4+}"–O and "Fe^{5+}"–O clusters.

The unit cell volume and, therefore, the Fe–O bond length (d) depends upon the size of the countercation. As will be described later, the present calculations reveal the importance of the bond length in such a point that the magnetic exchange interaction changes its sign at a critical bond length. However, the direct contribution of the countercations to the valence state is not important. Figure 3 displays the valence level structures of the FeO_6^{8-} and $Ca_8FeO_6^{8+}$ clusters, each having an Fe–O bond length of 1.887 Å. The up-spin and down-spin levels are split from each other by the spin polarization effect in either cluster. For the FeO_6^{8-} cluster, the levels whose main components are Fe $3d$ are the antibonding $2t_{2g}$ and $4e_g$ orbitals. The bonding counterparts are $1t_{2g}$ and $3e_g$, to which oxygen contributes mainly. It is noteworthy that $4e_g\uparrow$ and $2t_{2g}\uparrow$ sandwich a level to which oxygen mainly contributes. $2t_{2g}\uparrow$ are occupied and $4e_g\uparrow$ half occupied, while those for down-spin are all empty. This means that the Fe ion is in a high spin state of a formally $3d^4$ configuration. Cluster $Ca_8FeO_6^{8+}$ has a very similar level structure except the shallow core levels of Ca $3p$ and the excited states located above the Fe $3d$ levels. It may thus be said that the contribution of Ca^{2+} to

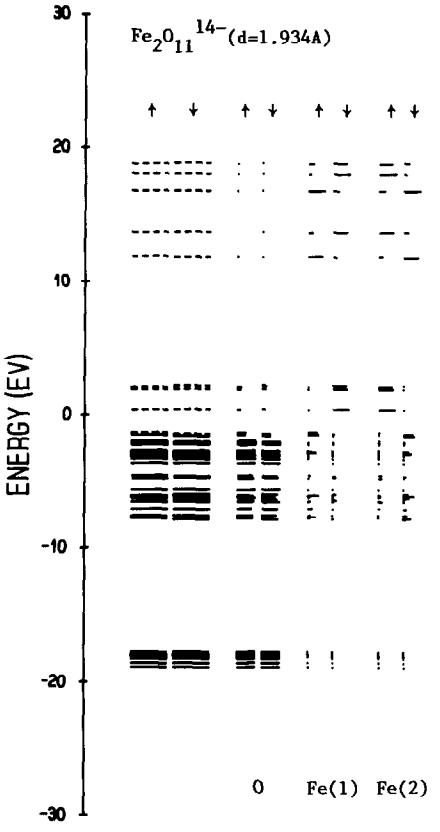

FIG. 6. Level structure of $Fe_2O_{11}^{14-}$ cluster with d = 1.934 Å. The antiferromagnetic exchange interaction can be clearly seen in the spin dependence of the Fe(1) and Fe(2) components.

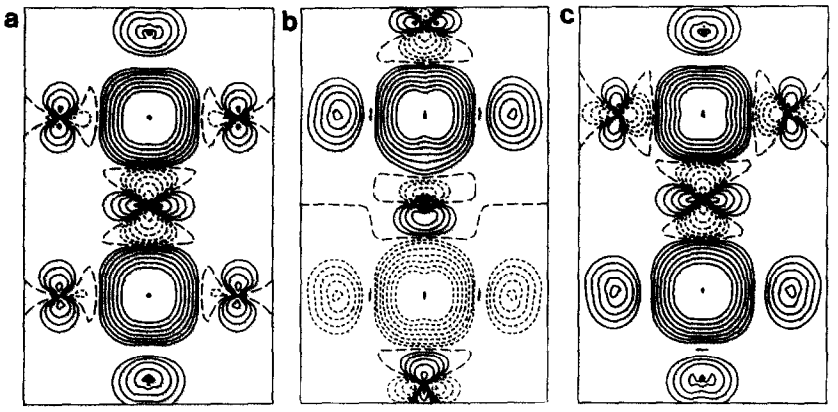

FIG. 7. Contour maps of the spin density for the $Fe_2O_{11}^{14-}$ cluster with (a) d = 1.887 Å, (b) d = 1.934 Å, and (c) d_1 = 1.940 Å, d_2 = 1.834 Å.

the valence level structure is very small. Calculations for $Sr_8FeO_6^{8+}$ with an Fe–O bond length appropriate to $SrFeO_3$ also showed similar results. According to Mulliken population analysis, the effective charges of the countercations are $Ca^{1.94+}$ and $Sr^{1.99+}$, which are very nearly the formal charge 2+.

The actual structure of $CaFeO_3$ is slightly distorted from cubic symmetry. Model cal-

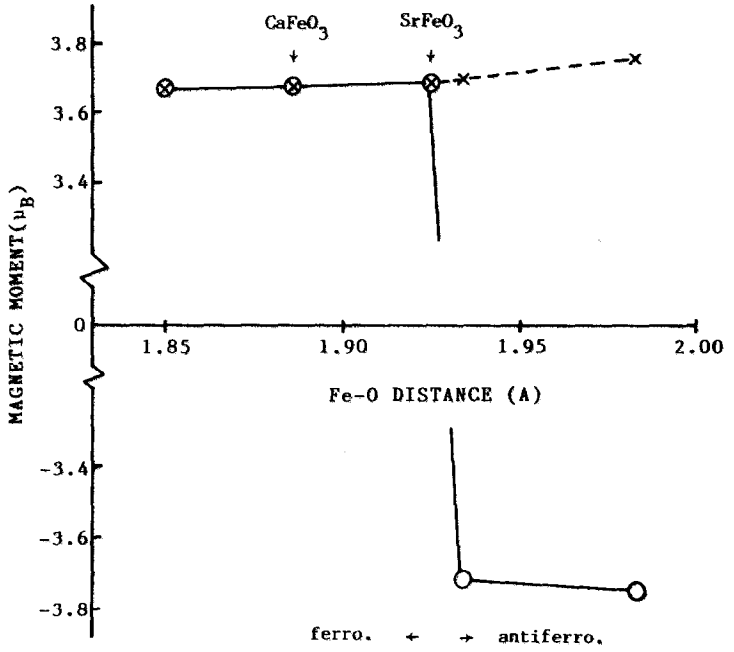

FIG. 8. Change in local magnetic moment on Fe^{4+} ions. (○) Fe(1), (×) Fe(2). The negative sign indicates the antiparallel spin arrangement.

culations for an FeO_6^{8-} cluster with D_{4h} symmetry did not reveal any significant change in the electronic structure, except small level splittings due to the distortion.

Next, we study the Fe–O–Fe interactions using the $Fe_2O_{11}^{14-}$ cluster shown in Fig. 1c with various Fe–O distances. Figure 4 represents the calculated level structure for d = 1.887 Å appropriate to $CaFeO_3$. In comparison with the structure for FeO_6^{8-} shown in Fig. 3, it is evident that covalent interactions between the two FeO_6 octahedra cause a considerable modification. The broadening of the O $2p$ band and the splitting of the "Fe $3d$" levels take place in the valence state. The most remarkable change is the splitting of one of the $4e_g$ levels into the $28a_1$ and $29a_1$ levels. As clearly seen from the contour maps of these orbitals shown in Fig. 5, the wave function for $29a_1\uparrow$ shows stronger antibonding interactions between the Fe $3d_{3z^2-r^2}$ and O $2p_z$ orbitals. The highest occupied level is $9b_1\uparrow$ and the lowest empty level is $10b_1\uparrow$. These are both of $3d_{x^2-y^2}$ parentage and are nearly degenerate. The electron configuration of each Fe^{4+} ion is thus essentially $t_{2g}^3e_g^1$ again. The level structure of the dimeric cluster with d = 1.925 Å appropriate to $SrFeO_3$ is similar, while at a larger value of d there occurs an interesting change in the magnetic interactions between the Fe^{4+} ions.

To determine the sign of the exchange interaction, we start the SCF iteration by assuming that one of the Fe^{4+} ions is in a high-spin state $d\uparrow^4 d\downarrow^0$ and the other one is in a nonmagnetic configuration $d\uparrow^2 d\downarrow^2$. Consequently, both Fe^{4+} ions have been found to remain in a high-spin state within the range of the Fe–O distance studied. The configuration according to the Mulliken population analysis is $d\uparrow^{4.44} d\downarrow^{0.77}$ for d = 1.887 Å and $d\uparrow^{4.47} d\downarrow^{0.78}$ for d = 1.925 Å, in good agreement with the results obtained for the single cluster mentioned above. Looking into Fig. 4, specifically the spin-dependence of the Fe(1) and Fe(2) components, one would notice that the two Fe ions are coupled ferromagnetically. However, it is evident in Fig. 6 that the level structure for d = 1.923 Å is quite different from those for d = 1.887 Å (Fig. 4) and 1.925 Å. The up- and down-spin valence levels are degenerate, while the former are mostly localized at Fe(1) and the latter at Fe(2). That is, for d = 1.934 Å the magnetic interaction is antiferromagnetic. The spin density maps for d = 1.887 and d = 1.934 Å are compared in Figs. 7a and 7b. Further calculations for d = 1.850 and 1.982 Å confirmed that the critical d value at which the magnetic interaction changes its sign is between 1.925 and 1.934 A. This prediction would be examined experimentally in the near future.

The local Fe magnetic moment can be estimated from the difference of the d orbital population between up- and down-spins. The value is typically 3.7 μ_B, increasing slightly with increasing d as illustrated in Fig. 8. A comparison between these calculated results with the experimental data will be done later.

As revealed by ME, a second-order disproportionation transition takes place at 290 K in $CaFeO_3$. CS and Hi are the spectroscopic parameters most sensitive to the d electron configuration, and from the experimental values the disproportionation has been expressed formally as $2Fe^{4+} \rightleftarrows Fe^{(4-\delta)+} + Fe^{(4+\delta)+}$, δ increasing from 0 toward 1 below the transition temperature. The transition has been presumed to be accompanied with quenching of the breathing phonon mode. However, usual powder X-ray diffraction has failed to detect the structural transition. One possibility is that the transition occurs in microdomains so that detected by X-ray diffraction is only the averaged symmetry. This is the reason why transmission electron microscopic studies are now being carried out at low temperatures. Anyway, in order to ascertain the breathing mode model theoretically, calculations have been made for dimeric clusters

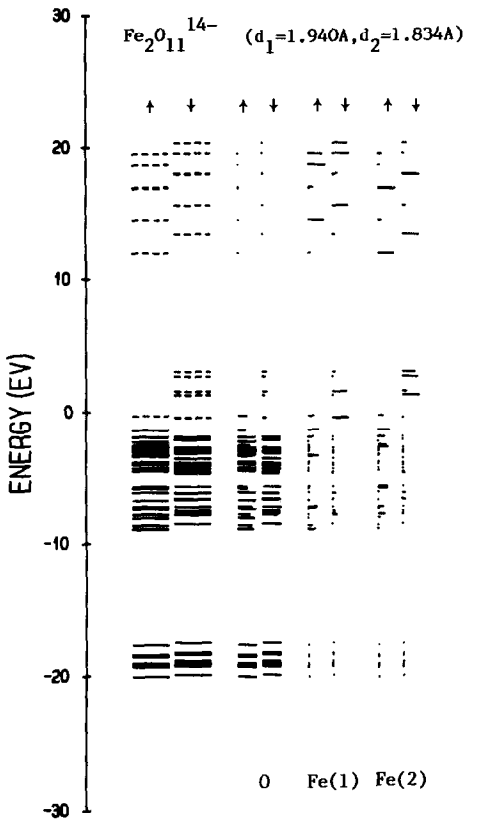

FIG. 9. Level structure of the model cluster for the charge disproportionated state of $CaFeO_3$.

in which the FeO distances of the two constituent octahedra are differentiated from d to $d_1 = d + \Delta$ and $d_2 = d - \Delta$.

The level structure for the cluster with $d_1 = 1.940$ Å and $d_2 = 1.834$ Å, or $d = 1.887$ Å and $\Delta = 0.053$ Å, is shown in Fig. 9. The most remarkable change in the electronic structure due to the differentiation of the bond length can be seen in Fig. 10, illustrating the highest occupied level $9b_1\uparrow$ and the lowest unoccupied level $10b_1\uparrow$. Levels $9b_1\uparrow$ and $10b_1\uparrow$ are, respectively, the bonding and antibonding states of a pair of orbitals of Fe(1) $d_{x^2-y^2}$ and Fe(2) $d_{x^2-y^2}$ parentage. The interactions between these orbitals are so weak that $9b_1\uparrow$ and $10b_1\uparrow$ are almost degenerate in the cluster with $d_1 = d_2$ ($\Delta = 0$), and each $9b_1\uparrow$ and $10b_1\uparrow$ has the same amplitude at the Fe(1) and Fe(2) sites by symmetry. In the cluster with $d_1 > d_2$, however, the amplitude of $9b_1\uparrow$ at Fe(1) with $d_1 = 1.940$ Å is larger than the amplitude at Fe(2) with $d_2 = 1.834$ Å and the amplitude of $10b_1\uparrow$ shows the reverse. This is because the Fe(1) $3d$ levels are lowered below those of Fe(2) after the distortion. Mainly by the reorganization of $9b_1\uparrow$, 0.28 of an up-spin electron is shifted from Fe(2) to Fe(1) (see Table II). This transfer is, however, counteracted by a partial (~0.19) transfer of a down-spin electron from Fe(1) to Fe(2). The counteraction is mainly due to a reorganization of the bonding partner occupied by down-spin electrons. So, the difference in spin density between Fe(1) and Fe(2) is considerably enhanced in comparison with the difference in the total d electron density.

The fact that $9b_1\uparrow$ and $10b_1\uparrow$ are almost degenerate is, from the viewpoint of the present model, the most essential point concerning the question why $SrFeO_3$ is metallic. It is expected that in $SrFeO_3$ an up-spin band as wide as ~1.7 eV ($E(29a_1\uparrow) - E(28a_1\uparrow)$) is formed and that the band is just half-filled. According to the present model, the semiconductive charge-disproportionated state

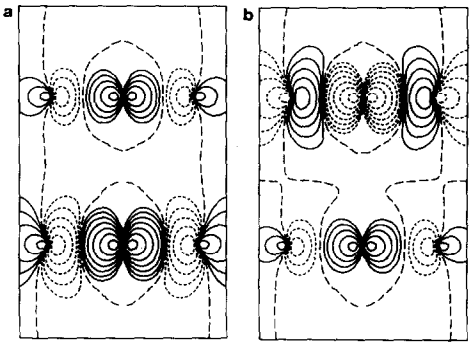

FIG. 10. Contour maps of the wave functions of the cluster with $d_1 = 1.940$ Å and $d_2 = 1.834$ Å. (a) $9a_1\uparrow$ and (b) $10b_1\uparrow$.

formally expressed as $2Fe^{4+} \rightleftarrows Fe^{(4-\delta)+} + Fe^{(4+\delta)+}$ of $CaFeO_3$ can be assigned to the reorganization of the $9b_1\uparrow$ orbital and the opening of a gap between $9b_1\uparrow$ and $10b_1\uparrow$. It was confirmed that both the degree of the reorganization and the gap width increase continuously as the difference in FeO bond length, 2Δ, increases. The half-filled band for $SrFeO_3$ with $\Delta = 0$ is split into a filled and an unfilled band for $\Delta > 0$, the gap width increasing with increasing Δ. As experimental data relevant to this we mention the composition dependence of the ME parameters for $Ca_{1-x}Sr_xFeO_3$ (*16*) and $Sr_{1-y}La_yFeO_3$ (*17*) and also the temperature dependence of CS for $CaFeO_3$ (*9, 10*). The differences in CS and Hi between the disproportionated components measured at 4 K for the two former systems decrease quite smoothly as Sr content increases. For $CaFeO_3$ the difference in CS between the disproportionated components increases continuously below 290 K to be saturated at 160 K. These results can be explained by assuming that Δ varies continuously as a function of Sr content and temperature. The results of Mulliken population analysis for the $Fe_2O_{11}^{14-}$ clusters are summarized in Table II.

A theoretical estimation of the Mössbauer parameters, CS and Hi, can be made by calculating the densities of up-spin and down-spin electrons at an iron nucleus, $\rho\uparrow(0)$ and $\rho\downarrow(0)$. The center shift can be estimated from the total electronic density at the nucleus $\rho(0) = \rho\uparrow(0) + \rho\downarrow(0)$ multiplied by the calibration constant which is assumed to be -0.30 as determined in previous work (*18*). The magnetic hyperfine field due to the Fermi contact interaction is obtained from the effective spin density at the nucleus $\Delta\rho\uparrow\downarrow(0) = \rho\uparrow(0) - \rho\downarrow(0)$. The values calculated for the model clusters for $CaFeO_3$ and $SrFeO_3$ are listed in Table III. These may generally be said to be in good agreement with the experimental data. As minor disagreements, the calculated difference in CS for $CaFeO_3$ is somewhat smaller than the experimental value and the calculated Hi values are somewhat larger. As already seen the electronic state is quite structure-sensitive, but the structure of Ca FeO_3 is not known in detail. The present calculations were performed nonrelativistically and within the framework of a point nucleus model, thus the quantitative accuracy of the calculated spin density at a nucleus is limited. The good agreement concerning the localized moment of $SrFeO_3$ seems to suggest the difficulty in the calculation of the hyperfine parameters caused by the limitation and the insufficient structural data.

The ferromagnetic nature of the Fe–O–Fe exchange interactions is in good agreement with the neutron diffraction study of $SrFeO_3$ made by Takeda *et al.* (*19*): They found a helical spin structure resulting from a competition of the ferromagnetic nearest-neighbor interaction with the antiferromagnetic second- and fourth-nearest neighbor interactions.

Acknowledgments

The authors thank the computer center of Institute for Molecular Sciences, Okazaki National Research Institute, for the use of a HITAC M-680H computer and also the computer center of Osaka University for the use of ACOS S2000 computers. This research was supported by a Grant-in-Aid for Scientific Research from Ministry of Education, Culture and Science.

References

1. J. B. MacChesney, R. C. Sherwood, and J. F. Potter, *J. Chem. Phys.* **43,** 1907 (1965).
2. F. Kanamaru, H. Miyamoto, Y. Miura, M. Koizumi, M. Shimada, and S. Sume, *Mater. Res. Bull.* **5,** 257 (1970).
3. Y. Takeda, S. Naka, M. Takano, T. Shinjo, T. Takada, and M. Shimada, *Mater. Res. Bull.* **13,** 61 (1978).
4. P. K. Gallagher, J. B. MacChesney, and D. N. E. Buchanan, *J. Chem. Phys.* **41,** 2429 (1964).
5. M. Takano, N. Nakanishi, Y. Takeda, S. Naka, and T. Takada, *Mater. Res. Bull.* **12,** 923 (1977).

6. M. TAKANO AND Y. TAKEDA, *Bull. Inst. Chem. Res. Kyoto Univ.* **61,** 406 (1983).
7. T. TAKEDA, S. KOMURA AND N. WATANABE, *in* "FERRITES: Proceedings of the International Conference September–October 1980, Japan" (H. Watanabe, S. Iida, and M. Sugimoto, Eds.), p. 385, Center for Academic Publication, Japan (1981).
8. T. TAKEDA, S. KOMURA, AND H. FUJII, *J. Magn. Magn. Mater.* **31–34,** 797 (1983).
9. M. TAKANO, N. NAKANISHI, Y. TAKEDA, AND S. NAKA, *J. Phys. Colloq.* **40,** C2–313 (1979).
10. T. SHINJO, N. HOSOITO, T. TAKADA, M. TAKANO AND Y. TAKEDA, "FERRITES: Proceedings of the International Conference September–October, 1980, Japan" (H. Watanabe, S. Iida, and M. Sugimoto, Eds.), p. 383, Center for Academic Publication, Japan (1981).
11. C. GLEITZER AND J. B. GOODENOUGH, *Struct. Bonding* **61,** 1 (1985).
12. H. ADACHI, M. TSUKADA, AND C. SATOKO, *J. Phys. Soc. Jpn.* **45,** 875 (1978).
13. H. ADACHI, S. SHIOKAWA, M. TSUKADA, C. SATOKO, AND S. SUGANO, *J. Phys. Soc. Jpn.* **47,** 1528 (1979).
14. C. SATOKO, M. TSUKADA, AND H. ADACHI, *J. Phys. Soc. Jpn.* **45,** 1333 (1978).
15. R. D. SHANNON, *Acta Crystallogr. Sect. A* **32,** 751 (1976).
16. Y. TAKEDA, S. NAKA, M. TAKANO, AND N. NAKANISHI, *J. Phys. Colloq.* **40,** C2-331 (1979).
17. M. TAKANO, J. KAWACHI, N. NAKANISHI, AND Y. TAKEDA, *J. Solid State Chem.* **39,** 75 (1981).
18. H. ADACHI, S. NASU, AND F. E. FUJITA, *Mater. Sci. Forum* **37,** 173 (1989).
19. T. TAKEDA, Y. YAMAGUCHI, AND H. WATANABE, *J. Phys. Soc. Jpn.* **33,** 967 (1972).